Tunable Conductivity of Collapsed Sandia Octahedral Molecular Sieves

Jason D. Pless,[†,§] Terry J. Garino,[†] James E. Maslar,[‡] and Tina M. Nenoff*[,†]

Sandia National Laboratories, P.O. Box 5800, MS-1415, Albuquerque, New Mexico 87185, and National Institute of Standards and Technology, 100 Bureau Drive Stop 8360, Gaithersburg, Maryland 20899-8360

Received April 25, 2007. Revised Manuscript Received July 25, 2007

The structure−property relationship between atomic cation substitution and bulk-scale conductivity in perovskites has been studied systematically. A series of Na−Nb perovskites has been synthesized via two methods, (1) ion exchange or (2) synthetic metal doping of microporous Sandia Octahedral Molecular Sieve (SOMS, $Na_2Nb_{2-x}M_xO_{6-x}(OH)_x{\cdot}H_2O$, where $0 \le x \le 0.4$) phases, followed by calcination to the perovskite phase. We show that the oxygen conductivity can be altered by substitution of the A- and B-site cations in the perovskite structure $Na_{1-x}A_xNb_{1-y}M_yO_{3-d}$, where $0 \le x \le 0.1$). Furthermore, we are able to show improved ion conductivity over that of yttria-stabilized zirconia with the $Na_{0.9}Mg_{0.1}Nb_{0.8}Ti_{0.2}O_{3-y}$ phase with our highest conductivity observed (0.176 S/cm) at 1173 K. These fundamental studies allow us to develop perovskites with optimal electric properties.

Introduction

Solid oxide fuel cells (SOFCs) offer several advantages over other types of fuel cells for the clean conversion of chemical energy into electricity. These advantages include flexible fuels (hydrocarbon-based), inexpensive non-noble-metal catalysts, and most importantly, high-efficiency conversion. The enhanced efficiency of SOFCs results from their high ionic mobility at elevated operating temperatures (1073−1273 K), allowing for high reaction rates and power densities.[1] However, technological difficulties arise at these operating temperatures: management of excess heat, the use of ceramic interconnects, thermal stresses, and component failure. Lowering the operating temperatures while maintaining high reaction rates and efficiency will help to overcome these problems.[2] To this end, a major materials breakthrough is needed to maintain or increase the high ionic mobility at lower temperatures.

Development of new solid electrolyte materials is not a straightforward or simple issue. New materials must possess ionic conductivities that are better than or similar to that of yttria-stabilized zirconia (8% YSZ, $\sigma = 0.10$ S/cm at 1273 K)[3] and be compatible with other fuel cell components. Perovskites, with the generalized compositions of ABO_3, exhibit high ionic conductivities and robust thermal stabilities and are being studied for use in SOFCs because of their ability to accommodate oxygen nonstoichiometries.[4] The ionic conductivity in these perovskites depends not only on the chemical composition but also on the extent of cation disorder. Traditional solid-state synthesis using oxide precursors requires high temperatures to form the desired perovskite phase(s). Alternatively, lower temperature hydrothermal perovskite synthesis methods could increase the available composition space by allowing the reaction to progress through novel metastable phase compositions resulting in perovskites with unique compositions and/or higher ion defect concentrations.[5−10] In addition, the Sandia Octahedral Molecular Sieve (SOMS) compositions can be altered through framework substitution of the niobium, initially shown with Ti and Zr,[5] and more fully explored and reported herein. Further compositional change can be facilitated

* To whom correspondence should be addressed. Phone: 505-844-0340. Fax: 505-844-5470. E-mail: tmnenof@sandia.gov.
† Sandia National Laboratories.
‡ National Institute of Standards and Technology.
§ Current address: Catalytic Solutions Inc., Oxnard, CA.

(1) Bagotzky, V. S.; Osetova, N. V.; Skundin, A. M. *Russ. J. Electrochem.* **2003**, *39*, 919−934.
(2) Steele, B. C. H.; Heinzel, A. *Nature* **2001**, *414*, 345−352.
(3) Minh, N. *J. Am. Ceram. Soc.* **1993**, *76*, 563−88.
(4) (a) Kindermann, L.; Das, D.; Bahadur, D.; Weiss, R.; Nickel, H.; Hilpert, K. *J. Am. Ceram. Soc.* **1997**, *80*, 909−914. (b) Ishihara, T.; Honda, M.; Shibayama, T.; Minami, H.; Nishiguchi, H.; Takita, Y. *J. Electrochem. Soc.* **1998**, *145*, 3177−3183. (c) Ullmann, H.; Trofimenko, N.; Tietz, F.; Stover, D.; Ahmad-Khanlou, A. *Solid State Ionics* **2000**, *138*, 79−90. (d) Thangadurai, V.; Weppner, W. *Ionics* **2002**, *8*. (e) Skinner, S. J. *Fuel Cells Bull.* **2004**, *4*, 6−12. (f) Orlovskaya, N.; Coratolo, A.; Johnson, C.; Gemmen, R. *J. Am. Ceram. Soc.* **2004**, *87*, 1981−1987. (g) Lepe, F. J.; Fernandez-Urban, J.; Mestres, L.; Martinez-Sarrion, M. L. *J. Power Sources* **2005**, *151*, 74−78.
(5) (a) Nyman, M.; Tripathi, A.; Parise, J. B.; Maxwell, R. S.; Harrison, W. T. A.; Nenoff, T. M. *J. Am. Chem. Soc.* **2001**, *123*, 1529−1530. (b) Nyman, M.; Tripathi, A.; Parise, J. B.; Maxwell, R. S.; Nenoff, T. M. *J. Am. Chem. Soc.* **2002**, *124*, 1704−1713. (c) Nenoff, T. M.; Nyman M. Niobate-based octahedral molecular sieves. U.S. Patent 6,596,254, July 22, 2003. (d) Nenoff, T. M.; Nyman M. Niobate-based octahedral molecular sieves. U.S. Patent 7,122,164, Oct 17, 2006.
(6) Iliev, M.; Phillips, M. L. F.; Meen, J. K.; Nenoff, T. M. *J. Phys. Chem. B* **2003**, *107*, 14261−14264.
(7) Xu, H.; Nyman, M.; Nenoff, T. M.; Navrotsky, A. *Chem. Mater.* **2004**, *16*, 2034−2040.
(8) Xu, H.; Navrotsky, A.; Nyman, M. D.; Nenoff, T. M. *J. Mater. Res.* **2005**, *20*, 618−627.
(9) Nenoff, T. M.; Pless, J. D.; Michaels, E. M.; Phillips, M. L. F. *Chem. Mater.* **2005**, *17*, 950−952.
(10) Ya, S.; Liyu, L.; Nenoff, T. M.; Nyman, M. D.; Navrotsky, A.; Xu, H. Investigation of SOMS and Their Related Perovskites. In *Nuclear Waste Management: Accomplishments of the Environmental Management Science Program*; Wang, P. W., Zachry, T., Eds.; ACS Symposium Series 943; American Chemical Society: Washington, DC, 2006; Chapter 15; pp 268−287.

10.1021/cm071122u CCC: $37.00 © 2007 American Chemical Society
Published on Web 09/12/2007

through ion exchange of the sodium cations in SOMS $Na_{2-x}A_xNb_{2-y}M_yO_{6-x}(OH)_x \cdot H_2O$, with $0 < x < 0.2$ and $0 < y < 0.4$. Therefore, we theorize that it is possible to synthesize compositions unobtainable through traditional methods using the metastable SOMS as a reactant for the synthesis of the perovskites.

It has been shown previously that heating metastable Sandia Octahedral Molecular Sieves (SOMS, $Na_2Nb_{2-x}M_xO_{6-x}(OH)_x \cdot H_2O$, where $0 \leq x \leq 0.4$ and M = Ti, Zr) phases at 723 K yields pure perovskite phases ($NaNb_{1-x}M_xO_{3-x}$, where $0 \leq x \leq 0.1$ and M = Ti, Zr).[5] Comparison of perovskites synthesized via low-temperature conversion of the SOMS phases with analogous perovskites made by high-temperature oxide heating shows that the low-temperature synthesis technique results in perovskites with lower exothermic heats of formation (ΔH).[11] (Similar results have been observed in condensed silicotitanates, where the ceramic phase "SNL-A" prepared hydrothermally is thermodynamically more stable than that prepared by solid-state methods.)[12] Comparison of literature data indicates that a lower ΔH may be an indicator of increased disorder on the crystallographic cation sites, which is desirable for enhanced ionic conductivity.[7,13]

The study reported herein investigates the structure−property relationship between these hydrothermally mediated perovskites and their resulting oxygen conductivities. The perovskites were synthesized from metastable SOMS precursors and their compositions were altered through framework substitution and/or ion exchange. Thermogravimetric analysis was used to determine the stability of the framework-substituted SOMS precursors. The perovskite structure was further investigated by powder X-ray diffraction, conductivity, Raman spectroscopy, and chemical analysis. We describe herein our results of the perovskite compositional phase space via the alternative low-temperature synthesis technique and the correlations between the phase composition, structure, and ionic conductivity.

Experimental Section

Synthesis. Titanium(IV) isopropoxide, $Ti(OCH(CH_3)_2)_4$ (Aldrich, 99.999%), molybdenum(V) isopropoxide, $Mo(OCH(CH_3)_2)_5$ (Alfa Aesar, 99+%), germanium isopropoxide, $Ge(OCH(CH_3)_2)_4$ (Aldrich, 97%), zirconium isopropoxide isoproponol complex, $Zr(OCH(CH_3)_2)_4 \cdot (CH_3)_2CHOH$ (Aldrich, 99.99%), niobium(V) ethoxide, $Nb(OC_2H_5)_5$ (Alfa Aesar, 99%), and tellurium(IV) isopropoxide, $Te(OCH(CH_3)_2)_4$ (Alfa Aesar, 99.9%), were purchased and handled as-received in an inert argon-filled drybox. Lithium nitrate, $LiNO_3$ (Aldrich, reagent plus), sodium hydroxide, NaOH (Alfa Aesar, 98%), magnesium chloride, $MgCl_2 \cdot 6H_2O$ (Aldrich, 99%), calcium chloride, $CaCl_2 \cdot 6H_2O$ (Aldrich, 98%), nickel(II) nitrate, $Ni(NO_3)_2 \cdot 6H_2O$ (Alfa Aesar, 98%), strontium chloride, $SrCl_2 \cdot 6H_2O$ (Aldrich, 99%), and yttrium chloride, $YCl_3 \cdot 6H_2O$ (99.9%), were used as-received. All reactions were carried out in solutions of deionized water.[14]

In a typical reaction, niobium ethoxide and a metal alkoxide were combined in a 4:1−20:1 ratio Nb:M in a 5 mL vial in an inert atmosphere drybox; total alkoxides was approximately 0.01 mol. The vial containing the alkoxide mixture was capped and removed from the drybox and treated ultrasonically to mix thoroughly. Sodium hydroxide was dissolved in 10 mL of deionized water in a 23 mL Teflon liner for a pressurized Parr reactor. The alkoxides were quickly added to the NaOH solution, and the resulting solution was shaken. The Teflon liner containing the aqueous mixture was placed inside a steel pressure reactor, sealed, and placed in an oven at 443 K for 4 h to 4 days. The resulting product was filtered and washed with 10 mL of deionized (DI) H_2O, and this process was repeated three times. The yield for a typical reaction is approximately 1.5 g or 90% yield based on the metal alkoxides.

Substitution of the sodium (both the channel and framework cations exchange out during the ion exchange process)[5] in the SOMS was accomplished via ion exchange using aqueous solutions of simple metals salts. In a typical exchange reaction, 1 g of SOMS was added to 25 mL of an aqueous solution of metal salt (2 equiv of metal per sodium) and stirred for 1 h at room temperature. The sample was filtered and washed with 10 mL of DI H_2O, and this process was repeated three times. The ion-exchange process was repeated two additional times. A more complete ion exchange was achieved by refluxing the SOMS sample in 25 mL of an aqueous solution of metal salt (2 equiv of metal per sodium) overnight.

Elemental analysis of all products was performed in duplicate by Galbaith Laboratories, Inc. Results are reported within the text.

Characterization. Powder X-ray diffraction (XRD) patterns were recorded at room temperature on a Siemens Kristalloflex D 500 diffractometer (Cu Kα radiation, Kevex detector, 40 kV, 30 mA; $2\theta = 5-60°$, 0.05° step size, and 3 s/step) and used for phase identification. The phases were refined and calculated by the JADE software least-squares method (see Table 1) and further identified by comparison with the data reported in the JCPDS (Joint Committee of Powder Diffraction Standards).[14]

Differential thermal analysis (DTA) and thermogravimetric analysis (TGA) of B-site substituted samples were performed on a TA Instruments STD 2960 Simultaneous DTA-TGA with alumina crucibles and alumina powder reference. The heating profile consisted of a 5 K/min linear ramp from ambient temperature to 1023 K in a static air atmosphere.

Raman spectra were obtained with 514.5 nm excitation (argon ion laser) using a custom-built Raman microprobe system. Incident laser radiation was delivered to the microprobe using a single-mode optical fiber and introduced into the microscope optical path using an angled dielectric edge filter in the so-called injection−rejection configuration. Collected scattered radiation was delivered to a 0.5 m focal length imaging single spectrograph using a multimode optical fiber. A 20× infinity-corrected microscope objective was used for focusing incident radiation and collecting scattered radiation. Power levels at the sample were less than 2 mW. Light was detected with a back-illuminated, charge-coupled device camera system operating at −90 °C. The instrumental band-pass (FWHM)

(11) Nenoff, T. M.; Xu, H. UC Davis, Davis, CA. Private communication, 2002.
(12) (a) Nyman, M.; Gu, B. X.; Wang, L. M.; Ewing, R. C.; Nenoff, T. M. *Microporous Mesoporous Mater.* **2000**, *40*, 115−125. (b) Nyman M.; Bonhomme, F.; Teter, D. M.; Maxwell, R. S., Gu, B. X.; Wang L. M.; Ewing, R. C.; Nenoff T. M. *Chem. Mater.* **2000**, *12*, 3449−3458. (c) Nyman, M.; Bonhomme, F.; Maxwell R. S.; Nenoff, T. M. *Chem. Mater.* **2002**, *13*, 4603−4611. (d) Nenoff, T. M.; Nyman, M. Cesium Silicotitanates for Ion Exchange and Waste Storage. U.S. Patent 6,-482,380, Nov 19, 2002.
(13) Xu, H.; Su, Y.; Balmer, M. L.; Navrotsky, A. *Chem. Mater.* **2003**, *15*, 1872−1878.

(14) Certain commercial equipment, instruments, and materials are identified in this publication to adequately specify the experimental procedure. Such identification in no way implies approval, recommendation, or endorsement by the National Institute of Standards and Technology, nor does it imply that the equipment, instruments, or materials identified are necessarily the best available for the purpose.

Table 1. Sample Compositions

compound	ion-exchange process	appearance	space group	unit cells (Å)
$NaNbO_3$	N/A	white	orthorhombic, *Pbma*	$a = 5.5563$ $b = 15.4733$ $c = 5.4933$ vol = 472.28
$NaNb_{0.948}Ti_{0.052}O_{2.974}$	N/A	white	orthorhombic, *Pbma*	$a = 5.5292$ $b = 15.2922$ $c = 5.5360$ vol = 460.09
$NaNb_{0.899}Ti_{0.101}O_{2.950}$	N/A	white	orthorhombic, *Pbma*	$a = 5.5778$ $b = 15.6715$ $c = 5.5167$ vol = 482.22
$NaNb_{0.845}Ti_{0.155}O_{2.923}$	N/A	white	orthorhombic, *Pbma*	$a = 5.5554$ $b = 15.6073$ $c = 5.5207$ vol = 478.67
$NaNb_{0.802}Ti_{0.198}O_{2.901}$	N/A	white	orthorhombic, *Pbma*	$a = 5.5367$ $b = 15.4859$ $c = 5.4848$ vol = 470.27
$NaNb_{0.866}Zr_{0.144}O_{2.928}$	N/A	white	orthorhombic, *Pbma*	$a = 5.5807$ $b = 15.6392$ $c = 5.5206$ vol = 481.82
$NaNb_{0.797}Mo_{0.203}O_{3-d}$	N/A	gray	monoclinic, *P*2/*m*	$a = 4.3456$ $b = 3.8989$ $c = 3.7747$ $\beta = 90.8°$ vol = 63.95
$NaNb_{0.807}Te_{0.193}O_{3-d}$	N/A	white	orthorhombic, *Pbma*	$a = 5.5723$ $b = 15.6286$ $c = 5.5536$ vol = 483.65
$Na_{0.655}Li_{0.345}Nb_{0.8}Ti_{0.2}O_{2.9}$	room temp	white	orthorhombic, *Pbma*	$a = 5.4789$ $b = 15.3298$ $c = 5.4943$ vol = 461.47
$Na_{0.855}Mg_{0.072}Nb_{0.78}Ti_{0.22}O_{2.89}$	room temp	white	orthorhombic, *Pbma*	$a = 5.5076$ $b = 15.3403$ $c = 5.5069$ vol = 465.27
$Na_{0.853}Ca_{0.065}Nb_{0.78}Ti_{0.22}O_{2.89}$	room temp	white	orthorhombic, *Pbma*	$a = 5.5282$ $b = 15.4163$ $c = 5.5322$ vol = 471.48
$Na_{0.890}Ni_{0.055}Nb_{0.8}Ti_{0.2}O_{2.9}$	room temp	light green	orthorhombic, *Pbma*	$a = 5.5102$ $b = 15.3395$ $c = 5.5236$ vol = 466.88
$Na_{0.88}Sr_{0.06}Nb_{0.78}Ti_{0.22}O_{2.89}$	room temp	white	orthorhombic, *Pbma*	$a = 5.5365$ $b = 15.4802$ $c = 5.5596$ vol = 476.49
$Na_{0.81}Sr_{0.095}Nb_{0.80}Ti_{0.2}O_{2.9}$	reflux	white	orthorhombic, *Pbma*	$a = 5.5371$ $b = 15.4797$ $c = 5.5646$ vol = 476.96
$Na_{0.91}Y_{0.045}Nb_{0.78}Ti_{022}O_{2.9}$	room temp	white	orthorhombic, *Pbma*	$a = 5.5342$ $b = 15.5386$ $c = 5.4825$ vol = 471.46

was approximately 4.1 cm^{-1}. All Raman intensities were corrected for the wavelength-dependent response of the optical system and by the factor of the square of the wavelength that is required in the transformation of the spectrum abscissa from the measured wavelength (in nanometer) to Raman shift expressed in wavenumber (cm^{-1}). The intensity correction was performed using NIST Standard Reference Material 2243 and as-described in the associated certificate of analysis.

Conductivities were measured using a four-point conductivity probe. The powders were pressed into pellets and heated at 1473 K in air for 1 h, to densify the samples (typically to >85% of theoretical density), and then cut into bars (nominally 2 mm × 2

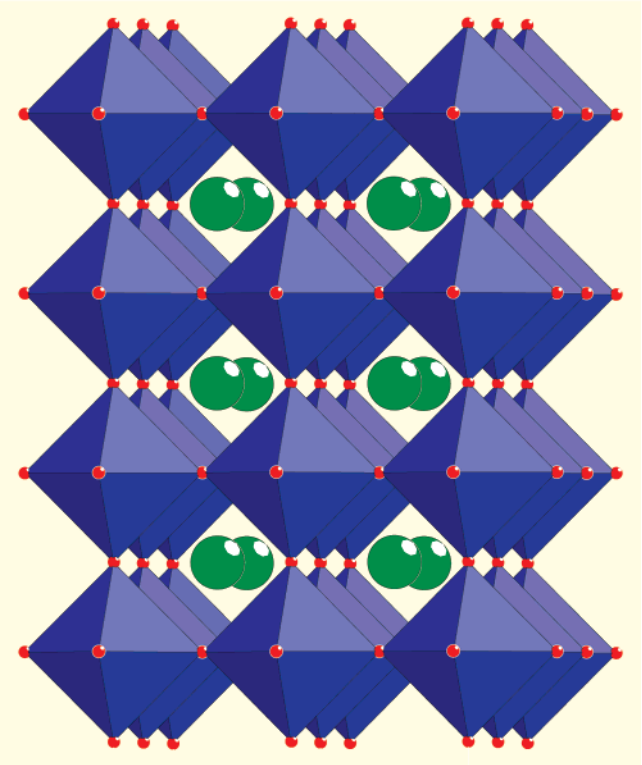

Figure 1. ABO_3 perovskite crystal structure: A = green balls; B = blue octahedral; O = small red balls.

mm × 20 mm). Platinum wires were then attached at four spots with conductive silver-palladium paste to ensure good electrical conduction between the wires and the sample. The samples were placed in a tube furnace with a dc current source connected to two wires and a voltmeter connected to the other two wires to measure the voltage drop across the sample. The measurements were made in air between 773 and 1173 K. Select samples were measured in varying pO_2 atmospheres (e.g., UHP Ar and 3% H_2 in Ar) to help determine the nature of the conductivity (ionic or electronic). The conductivity was calculated from the current, voltage, and geometry of the sample and compared against measurements made on 3% YSZ, which has a conductivity similar to that of the commonly used 8% YSZ.[15]

Results and Discussion

To understand the structure/property relationship between oxygen conductivity and perovskite composition, it is necessary to understand the perovskite structure, ABO_3 (Figure 1).[16] The perovskite structure can be described as a cube comprised of eight BO_6 octahedra with the 12-coordinate A-site cation located in the cube's center. In an undistorted cubic perovskite the A-site cations substitute 25% of the oxide anions of a perfect fcc lattice. Therefore, the oxide anions must migrate through a triangular space consisting of two large A-site cations and one smaller B-site cation. The enlargement of this triangular space facilitates the migration of O^{2-} ions through the crystal lattice. Thus, the oxygen conductivity of cubic ABO_3 perovskites is dependent more on the size of the A-site cation and less so on the size of the B-site cation. Therefore, higher oxygen conductivities are expected from cubic perovskites that contain larger lattice parameters. However, if the A-site cation is increased, then the "free" volume that the oxygen anion can migrate through decreases. For example, thermal treatment of the SOMS to form perovskite can be written as

$$A_2Nb_{2-x}M_xO_{6-x}(OH)_x \cdot H_2O \rightarrow ANb_{1-x}M_xO_{3-\delta} \qquad (1)$$

in which resultant oxygen vacancies would affect material conductivity. Furthermore, examples of phases that can be studied for direct observation between the A-site cation of the perovskite structure and the conductivity data include $Na_{0.9}Mg_{0.1}Nb_{0.8}Ti_{0.2}O_3$ and $Na_{0.9}Sr_{0.1}Nb_{0.8}Ti_{0.2}O_3$ or $NaNbO_3$ and $Na_{0.9}Sr_{0.2}Nb_{0.8}Ti_{0.2}O_3$. Similarly, the conductivity can be increased by the incorporation of cation vacancies on the A-site, which enlarges the triangular space that the oxygen migrates through. The perovskite structure can stabilize at least 10% cation vacancies on the A-site.[17] It is expected that an increase in conductivity would be observed upon the incorporation of a small trivalent cation (i.e., Al or Ga) on the A-site. Any positive benefit in conductivity from the substitution of larger trivalent cations (Y or La) would be negatively compensated for by the decrease in space that the oxide ion must travel through.

Perovskite Precursor Synthesis. The hydrothermal synthesis described in the Experimental Section produced single-phase microcrystalline powder samples with the microporous SOMS structure. Framework substitutions of Nb by M (M = Mo, Te, Zr, Ge, Ti) were made to study a variety of factors on the conductivities of the perovskite structure (Table 1). The factors studied include ionic radii, redox potential, stereochemically active lone pair of electrons of M, and metal concentrations. The resulting structure and purity are dependent upon the reaction time and consistent with previous studies.[5a,5b]

With increasing reaction time, the aqueous inorganic phases crystallize into higher order structures. Ex situ X-ray diffraction studies (Figure 2) show that the reaction proceeds from solution to a one-dimensional anionic cluster (the sodium hexaniobate ($Na_7(H_3O)(Nb_6O_{19})(H_2O)_{14}$)),[5] to the ordered three-dimensional microporous SOMS, and then to the condensed three-dimensional orthorhombic perovskite structure ($NaNbO_3$) with space group *Pbma*. Exceptions are the Ge and Zr alkoxide mixtures in which an intermediary layered two-dimensional hexagonal ilmenite-like phase ($NaNbO_3$, space group $R\bar{3}$)[18] crystallizes in solution prior to formation of the perovskite phase. In particular, the reaction time is dependent upon the amount of Ti substitution; the reaction time increased with increasing Ti substitution.[5]

Ion exchange was performed to study how various A-site cations affect the conductivity of the perovskite. Single-phase 20% Ti-SOMS, with its reproducible crystallinity,[5] was chosen for the substitution of various cations onto the exchangeable sodium sites in the SOMS structure. Cation-exchange reactions with Li^+, Mg^{2+}, Ca^{2+}, Ni^{2+}, Sr^{2+}, and Y^{3+} were performed to ascertain how the conductivity is

(15) Lee, Y. K.; Park, J. W. *J. Mater. Sci. Lett.* **1997**, *16*, 678−682.
(16) Cotton, F. A.; Wilkinson, G.; Murillo, C.; Bochmann, M. *Advanced Inorganic Chemistry*, 6th ed.; Wiley: New York, 1999.
(17) Zheng, H.; Reaney, I. M.; de Gyorgyfalva, G.; Ubic, R.; Yarwood, J.; Seabra, M. P.; Ferreira, V. M. *J. Mater. Res.* **2004**, *19*, 488−495.
(18) Kumada, N.; Kinomura, N.; Muto, F. *Nippon Seramikkusu Kyokai Gakujutsu Ronbunshi* **1990**, *98*, 384−388.

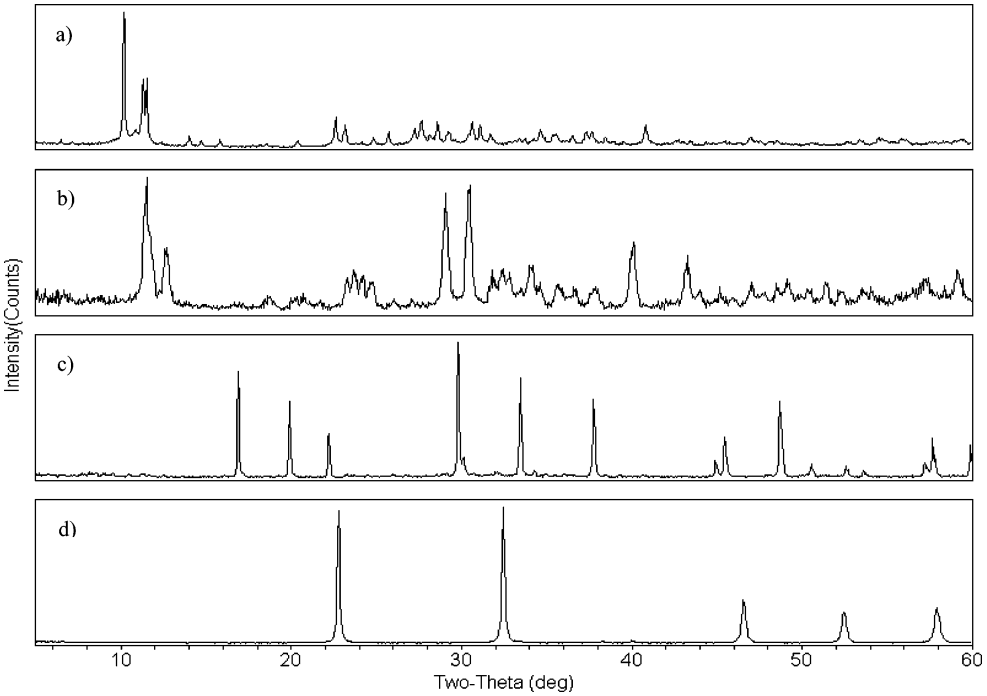

Figure 2. Ex situ X-ray diffraction patterns of the (a) hexaniobate, (b) SOMS, (c) ilmenite-like, and (d) perovskite structures formed with time under hydrothermal conditions (increasing time from top to bottom frame), with <1 h interval between each sample.[5a,b]

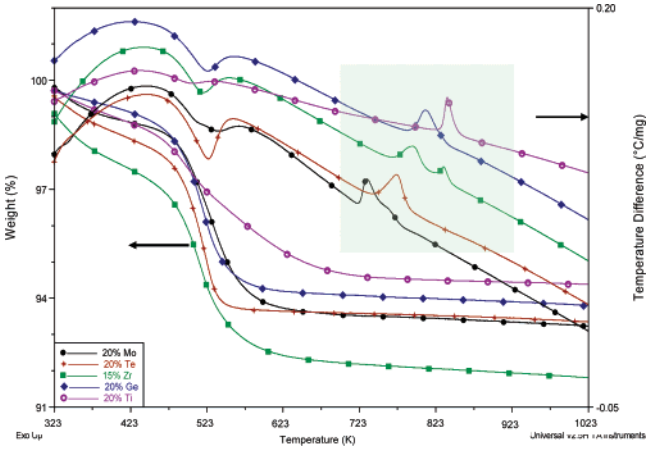

Figure 3. Thermogravimetric and differential scanning calorimetry data of framework-substituted SOMS phases.

modified by ionic radii, charge-size ratio, and redox properties. Ion exchange with Fe^{3+}, Mn^{3+}, and Co^{2+} resulted in a mixture SOMS and perovskites. No further characterization was performed on these mixed-phase samples because of their phase heterogeneity. Room-temperature ion exchange resulted in approximately 10 mol % exchange of the sodium ions (see Table 1). A complete exchange of the Na^+ (20 mol %)[5a] was accomplished by ion exchange under reflux at 363 K. The different amounts of ion exchange allow us to determine how the A-site cation concentration affects the conductivity.

Perovskite Formation. Figure 3 shows the TGA/DTA curves for the framework-substituted SOMS phases. An endothermic peak is observed near 523 K and the corresponding weight loss is associated with evaporation of the occluded water.[5] An exothermic peak is observed between 723 and 873 K, depending upon the framework-substituted element and this peak indicates the transformation from the microporous SOMS structure to the dense perovskite phase.[5] The range in temperatures for the structural transformation indicates that the thermal stability of the SOMS phase is directly affected by the type of substituting element. The Mo−SOMS is the least stable and transforms to perovskite at the lowest temperature 731 K; conversely, Ti−SOMS is most the stable and transforms to perovskite at the highest temperature 833 K. This trend is consistent with previous results.[5]

The DTA of the Mo− and Zr−SOMS show a second, less intense peak at higher temperatures (746 and 833 K, respectively). The samples were heated and cooled to intermediate temperatures. Ex situ XRD studies were then performed to identify if any additional phases formed; the data indicated that only orthorhombic perovskite is present, and no secondary phase formed.

In consideration of the thermogravimetric analysis, fifteen single-phase SOMS compositions were calcined at 1073 K. Examination of the powder diffraction patterns reveals the formation of the pure orthorhombic perovskite phases (Figure 4); there is no evidence of a secondary phase for the Ni-substituted sample, but the ionic radius suggests that Ni^{2+} would not fit on the A-site.[19] (In addition, the peak at ≈30.8° (2θ) is observed in the $Na_{0.9}Mg_{0.1}Nb_{0.8}Ti_{0.2}O_{2.9}$ sample and could not be indexed to any known phase; this peak observed with the smaller peak at ≈10.5° might signify unconverted SOMS phase.) The product sample compositions are listed in Table 1. These samples were used for further analysis.

Raman Characterization. Figure 5 shows the Raman spectra of the $NaNbO_3$, $NaNb_{0.8}Ti_{0.2}O_{2.9}$, and $Na_{0.9}Mg_{0.1}Nb_{0.8}Ti_{0.2}O_{2.95}$ powders. The Raman spectrum of $NaNbO_3$ exhibits two relatively intense groups of peaks in the 200 to ≈350 cm^{-1} range and ≈500 to ≈700 cm^{-1} range, as well as weaker

(19) Shannon, R. D.; Prewittt, C. T. *Acta Crystallogr.* **1969**, *B25*, 925−946.

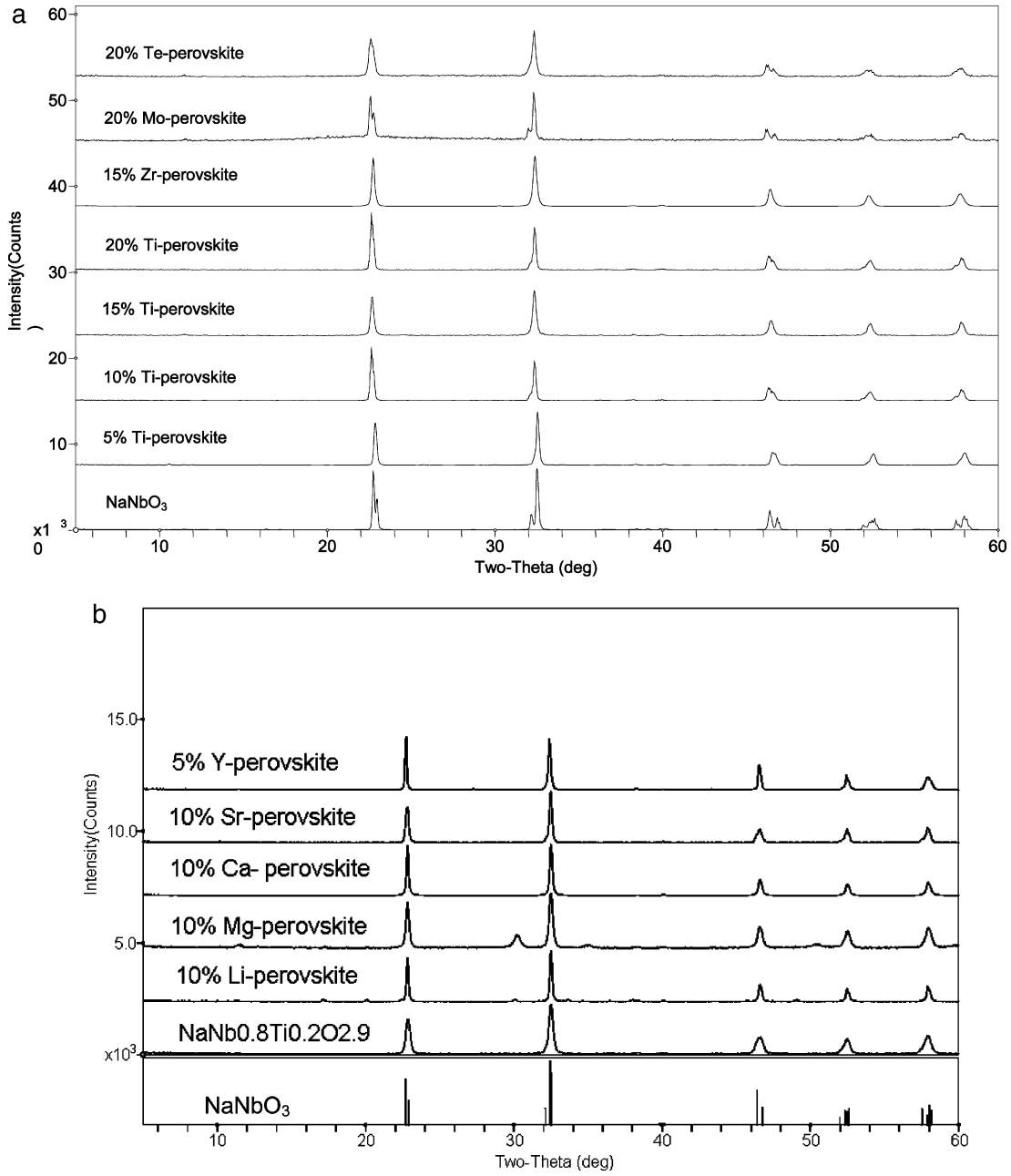

Figure 4. X-ray diffraction patterns of (a) framework-substituted perovskites and (b) ion-exchanged $NaNb_{0.8}Ti_{0.2}O_{2.9}$.

features at ≈378, ≈435, and ≈872 cm^{-1}. For simplicity, all these peaks are often assigned in terms of the internal modes of the [NbO_6] octahedra,[20,21] although this description of the $NaNbO_3$ lattice dynamics is not strictly accurate. The Raman spectra of $NaNb_{0.8}Ti_{0.2}O_{2.9}$ and $Na_{0.9}Mg_{0.1}Nb_{0.8}Ti_{0.2}O_{2.95}$ also exhibit relatively intense features in the 200 to ≈350 cm^{-1} range and ≈500 to ≈700 cm^{-1} range. The overall similarity of these three spectra indicates that the structures of the $NaNb_{0.8}Ti_{0.2}O_{2.9}$ and $Na_{0.9}Mg_{0.1}Nb_{0.8}Ti_{0.2}O_{2.95}$ powders are closely related to that of $NaNbO_3$. However, differences are evident between the $NaNbO_3$ spectrum and the $NaNb_{0.8}Ti_{0.2}O_{2.9}$ and $Na_{0.9}Mg_{0.1}Nb_{0.8}Ti_{0.2}O_{2.95}$ spectra as well as between the $NaNb_{0.8}Ti_{0.2}O_{2.9}$ and $Na_{0.9}Mg_{0.1}Nb_{0.8}Ti_{0.2}O_{2.95}$ spectra, indicating some variation in the respective structures.

The $NaNb_{0.8}Ti_{0.2}O_{2.9}$ and $Na_{0.9}Mg_{0.1}Nb_{0.8}Ti_{0.2}O_{2.95}$ spectra exhibit fewer resolved peaks on the relatively intense 200 to ≈350 cm^{-1} and ≈500 to ≈700 cm^{-1} features compared to the $NaNbO_3$ spectrum. The resolution of fewer peaks is attributed to a general peak broadening and concomitant loss of peak resolution due to the substitution of (1) titanium or magnesium and (2) titanium into the $NaNbO_3$ lattice. In addition to the relatively intense features observed in the $NaNbO_3$ spectrum, the $NaNb_{0.8}Ti_{0.2}O_{2.9}$ spectrum exhibits a relatively broad, moderately intense feature at ≈878 cm^{-1} with a weaker shoulder at ≈848 cm^{-1} and very weak features at ≈495 and ≈745 cm^{-1}, while the $Na_{0.9}Mg_{0.1}Nb_{0.8}Ti_{0.2}O_{2.95}$ spectrum exhibits a moderately intense feature at ≈879 cm^{-1} and weak features at ≈495 and ≈728 cm^{-1}. Assuming that

(20) Shen, Z. X.; Wang, X. B.; Tang, S. H.; Kuok, M. H.; Malekfar, R. *J. Raman Spectrosc.* **2000**, *31*, 439−443.
(21) Shiratori, Y.; Magrez, A.; Dornseiffer, J.; Haegel, F. H.; Pithan, C.; Waser, R. *J. Phys. Chem. B* **2005**, *109*, 20122−20130.

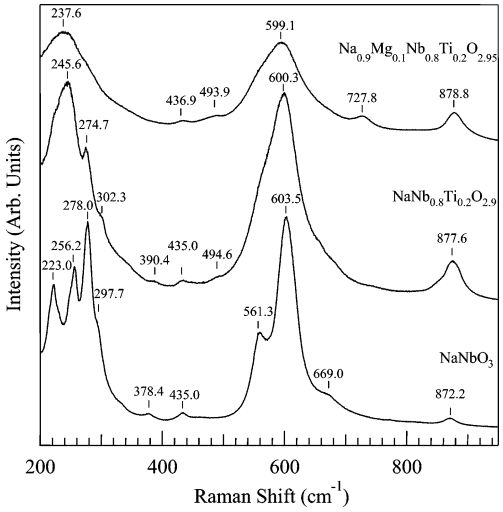

Figure 5. Raman spectra of the $NaNbO_3$, $NaNb_{0.8}Ti_{0.2}O_{2.9}$, and $Na_{0.9}Mg_{0.1}Nb_{0.8}Ti_{0.2}O_{2.95}$ powders. The spectra are offset on the vertical scale for clarity.

these materials are predominantly single phase, the additional weak features in the $NaNb_{0.8}Ti_{0.2}O_{2.9}$ and $Na_{0.9}Mg_{0.1}Nb_{0.8}Ti_{0.2}O_{2.95}$ spectra compared to those in the $NaNbO_3$ spectrum are attributed to structural modifications associated with substitution of (1) titanium or (2) titanium and magnesium into the $NaNbO_3$ lattice.

$NaNb_{0.8}Ti_{0.2}O_{2.9}$ and $Na_{0.9}Mg_{0.1}Nb_{0.8}Ti_{0.2}O_{2.95}$ are structurally complex and a detailed understanding of the lattice dynamics of these materials is lacking. Hence, it is impossible to assign the spectral features with certainty and only tentative assignments will be made in this report. Peaks in the ≈700 to ≈900 cm^{-1} range in perovskite materials have been widely observed and are attributed to $[BO_6]$ breathing-related modes.[17,22,23] Such modes are symmetry-forbidden for ideal cubic perovskite structures but are Raman-active for perovskite structures with lower crystal symmetry, e.g., due to distortion of the $[BO_6]$ octahedra and/or the presence of multiple B-site cations.[17,24] In complex perovskites, only features associated with $[BO_6]$ breathing modes are typically observed in the ≈700 to ≈900 cm^{-1} range. Hence, the features at ≈878, ≈848, and ≈745 cm^{-1} in the $NaNb_{0.8}Ti_{0.2}O_{2.9}$ spectrum and at ≈879 and ≈728 cm^{-1} in the $Na_{0.9}Mg_{0.1}Nb_{0.8}Ti_{0.2}O_{2.95}$ spectrum are attributed to $[BO_6]$ breathing modes. The observation of multiple $[BO_6]$ breathing modes in these spectra indicates that multiple $[BO_6]$ octahedra types are present in these structures, as expected for complex perovskites.[22,25,26] The ≈870 cm^{-1} peak in the Raman spectra of $LiNbO_3$ and $NaNbO_3$ powders has been assigned to a stretching mode of the Nb−O−Nb linkage that is Raman-active due to tilting of the $[NbO_6]$ octahedra.[24] Given the wavenumber of this mode, it seems likely that this mode is more specifically related to the $[NbO_6]$ breathing mode. The close wavenumber correspondence of the ≈878 cm^{-1} peak in the $NaNb_{0.8}Ti_{0.2}O_{2.9}$ spectrum and the ≈879 cm^{-1} peak in the $Na_{0.9}Mg_{0.1}Nb_{0.8}Ti_{0.2}O_{2.95}$ spectrum to the ≈872 cm^{-1} peak in the $NaNbO_3$ spectrum indicates that all of these peaks correspond to a similar, although slightly modified, vibrational mode. Hence, the ≈878 cm^{-1} peak in the $NaNb_{0.8}Ti_{0.2}O_{2.9}$ spectrum and the ≈879 cm^{-1} peak in the $Na_{0.9}Mg_{0.1}Nb_{0.8}Ti_{0.2}O_{2.95}$ spectrum are attributed to the $[NbO_6]$ breathing mode that is Raman-active due to distortion of the $[NbO_6]$ octahedra. The difference in wavenumber of the ≈848 cm^{-1} feature from the ≈878 cm^{-1}/≈879 cm^{-1} peaks indicates that the $[BO_6]$ octahedra responsible for this feature are either chemically different from $[NbO_6]$, e.g., $[TiO_6]$,[22] and/or exist in a different vibrational environment than the octahedra responsible for the ≈878 cm^{-1}/≈879 cm^{-1} peaks.[25] The lack of detailed structural information for these materials makes it impossible to identify the origin of the ≈848 cm^{-1} feature. However, if one assumes single-phase materials of related perovskite structure, the observation of this feature in only one spectrum suggests that it is not directly related to B-site cation distribution since the niobium/titanium distribution is expected to be nominally the same in both materials (whether the distribution is disordered or ordered). Assuming that this is the case, it is reasonable to speculate that the disappearance of the ≈848 cm^{-1} feature in the $Na_{0.9}Mg_{0.1}Nb_{0.8}Ti_{0.2}O_{2.95}$ spectrum is related to the addition of magnesium to the $NaNb_{0.8}Ti_{0.2}O_{2.9}$ lattice and the effects upon the structure associated with the different size and/or charge of magnesium with respect to sodium.

With the above assumptions, the disappearance of the ≈848 cm^{-1} feature in the $Na_{0.9}Mg_{0.1}Nb_{0.8}Ti_{0.2}O_{2.95}$ spectrum suggests that the addition of magnesium leads to less octahedra distortion in $Na_{0.9}Mg_{0.1}Nb_{0.8}Ti_{0.2}O_{2.95}$ than in $NaNb_{0.8}Ti_{0.2}O_{2.9}$. The observation of the ≈745 cm^{-1}/≈728 cm^{-1} $[BO_6]$ breathing mode in both spectra but at a weak intensity suggests that this feature is related to the titanium cation since titanium is present at nominally the same dilute concentration in both materials. If so, this mode is possibly a so-called localized mode involving solute $[TiO_6]$ octahedra.[22] The weak feature at ≈495 cm^{-1} in the $NaNb_{0.8}Ti_{0.2}O_{2.9}$ and $Na_{0.9}Mg_{0.1}Nb_{0.8}Ti_{0.2}O_{2.95}$ spectra is attributed to a mode analogous to either a Ti−O torsional mode in $CaTiO_3$[17] or an oxygen vibration normal to the Ti−O−Nb bond axis in $Ca(Al_{0.5}Nb_{0.5})O_3$−$CaTiO_3$ solid solutions,[22] the wavenumbers of these modes being observed in the 470 to 494 cm^{-1} range.

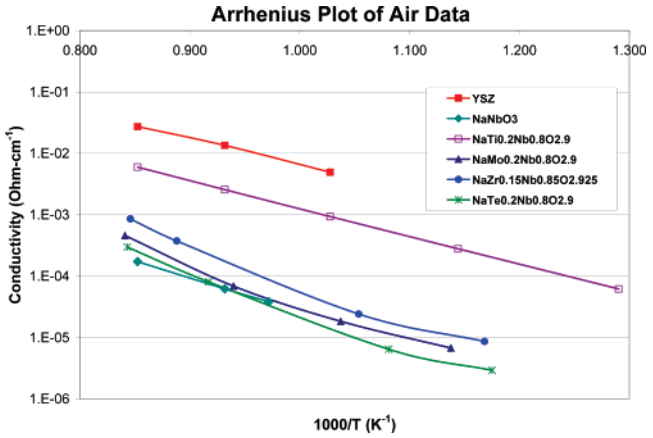

Figure 6. Conductivities for various B-site substituted perovskites.

(22) Levin, I.; Cockayne, E.; Lufaso, M. W.; Woicik, J. C.; Maslar, J. E. *Chem. Mater.* **2006**, *18*, 854−860.
(23) Seabra, M. P.; Ferreira, V. M.; Zheng, H.; Reaney, I. M. *J. Appl. Phys.* **2005**, *97*.
(24) Jehng, J. M.; Wachs, I. E. *Chem. Mater.* **1991**, *3*, 100−107.
(25) Blasse, G.; Corsmit, A. F. *J. Solid State Chem.* **1974**, *10*, 39−45.
(26) Levin, I.; Chan, J. Y.; Maslar, J. E.; Vanderah, T. A.; Bell, S. M. *J. Appl. Phys.* **2001**, *90*, 904−914.

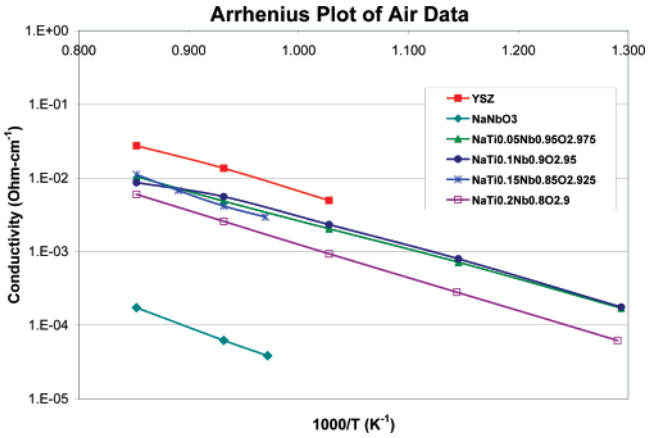

Figure 7. Conductivities for varying concentrations of Zr and Ti (B-site) substituted perovskites.

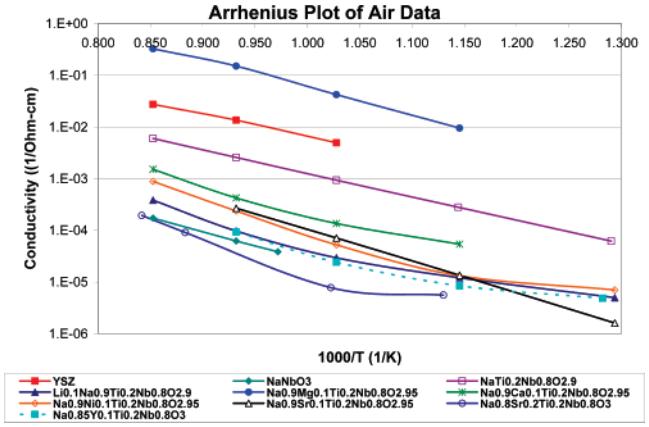

Figure 8. Conductivities for various A-site substituted perovskites.

Conductivity. The conductivities of all the perovskite samples are presented in Figures 6−9 with the conductivity of 3% yttria stabilized (YSZ) used as a reference. The measured conductivity of $NaNbO_3$ (1.73×10^{-4} S/cm) is 2 orders of magnitude smaller than YSZ (1.73×10^{-2} S/cm) at 1173 K. These data indicate that the conductivity of $NaNbO_3$ is affected by both the substitution of various transition metals for the niobium into the framework structure (Figure 6) and by ion exchange of the Na atoms (Figure 8). In addition, the amount of metal substitution into the framework also affects the conductivity (Figure 7), thus implicating atomic-scale variations and their effects on the perovskite's bulk properties.

An improvement in the conductivity was observed upon the substitution of Ti, Zr, Mo, or Te into the Nb site. The corresponding conductivities of the substituted $NaNbO_3$ increase as a function of the substitution of the tetravalent cation into the niobium site. This behavior is consistent with the oxygen ion being responsible for the bulk of the conductivity since these substitutions will create oxygen vacancies to balance charge, and the oxygen ion conductivity is directly proportional to the oxygen vacancy concentration.

The Te and Mo substituted phases did not have the expected high increase in conductivity. We postulate this is because of the stereochemically active lone pair of electrons of the Te^{4+} ions; these stereochemically active lone pairs would repel the negatively charged oxide anions and thereby impede their migration. In the case of Mo, the +6 oxidation

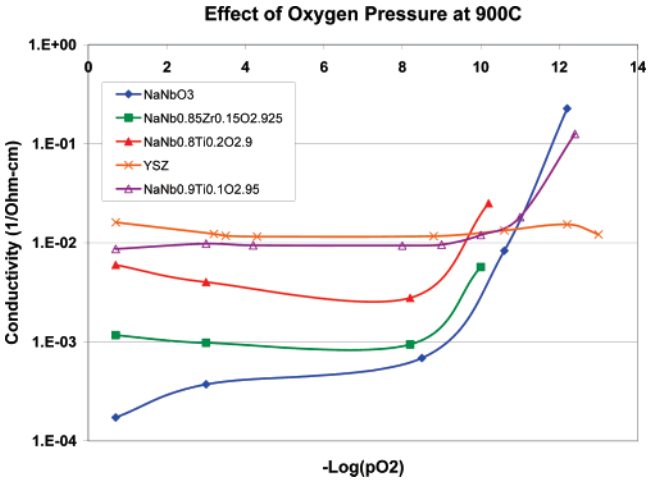

Figure 9. Conductivity versus oxygen partial pressure for select perovskites.

state is more stable than Mo^{4+}, which would incorporate additional oxygen atoms into the structure and thereby detrimentally affect the conductivity of oxygen. Ongoing titration studies are being performed to determine the oxidation states of both the Te and Mo in these perovskites.[4,5]

Additional studies were performed to determine the affect of varying amounts of substitution on the niobium sites (Figure 7). A significant increase in the conductivity is observed when the Ti substitution is decreased to 15 mol %. This correlates to a marked increase in the stabilization of the perovskite structure, with respect to ΔH of these perovksites.[13] Additional small improvements in the conductivity (and perovskite structure stability) are observed upon decreasing the amount of substitution.[13] If the thermodynamic data is only considered, one would expect that the conductivity of $NaNbO_3$ would be higher than all of the Ti^{4+} substituted perovskites. However, we postulate that the lack of oxygen vacancies in the unsubstituted $NaNbO_3$ impedes oxygen mobility and so no increase in conductivity is observed.

Oxygen conductivity was also affected by the substitution of Na atoms (A-site cation) by various metals (Figure 8). The conductivity of the alkaline earth metal perovskites increases with increasing basicity or increasing charge to size ratio of the cation. The $Na_{0.9}Mg_{0.1}Nb_{0.8}Ti_{0.2}O_{3-y}$ sample exhibits the highest conductivity (0.176 S/cm at 1173 K), which is an order of magnitude higher than that measured for 3% YSZ. However, a decrease in the conductivity was observed in all the other ion-exchanged 20% Ti−SOMS derived perovskites samples. We speculate that the decrease in conductivity results from the destruction of the oxygen vacancies because of the charge compensation from the substitution of divalent cations for the monovalent sodium ion. Supporting evidence for this theory is observed in the decrease in conductivity for the $Na_{0.8}Sr_{0.2}Nb_{0.8}Ti_{0.2}O_3$ compared to that for the $Na_{0.9}Sr_{0.1}Nb_{0.8}Ti_{0.2}O_3$; there should be net charge compensation from the divalent Sr^{2+} ion exchange.

The conductivities of select compositions were measured isothermally at various oxygen partial pressures to determine if the conductivity was ionic or electronic (Figure 9). Ionic conductivities are independent of the oxygen pressure while

electronic conductivity varies with oxygen pressure.[27] The linearity of the plots confirms the primarily ionic nature of the conductivity. The sharp increase in conductivity at $pO_2 < 10^{-8}$ results from the reduction of the sample.

Regarding the nature of the ion in these materials, results suggest that the mobile ion in these materials is oxygen. The activation energy for conduction of the samples was in the same range as that for oxygen conduction in YSZ materials. All conductivity measurements were performed at equilibrium. There was no decrease in the dc conductivity with time, as would occur due to polarization of a different ion, such as sodium, being the mobile species.

Conclusions

The use of the SOMS structure as a metastable reactant phase is an alternative route for synthesizing perovskites for use as ionic conductors. This low-temperature synthetic route allows for a large compositional phase space to be studied by changing the concentration and type of the A- and B-site cations. Structure−property relationships between substituted phases can be monitored by both thermal analyses and Raman spectroscopy. Changes in Raman wavenumber shift and relative signal-to-noise ratios of features in the respective spectra with similar origin are attributed to differences in octahedra distortion and/or lattice strain between the respective materials. In particular, substitution into the A-site by replacement of some Na with Mg results in a decreased distortion than nonsubstituted analogs. The conductivity of $NaNbO_3$ was found to increase with the creation of oxygen vacancies formed for charge compensation upon substitution of M^{4+} for Nb^{5+}. In addition, the conductivity correlates with the charge to size ratio of the substituting A-site cation. To date, the $Na_{0.9}Mg_{0.1}Nb_{0.8}Ti_{0.2}O_{3-\delta}$ shows the best conductivity, with an approximate 1 order of magnitude improvement over YSZ. Ongoing thermodynamic studies will measure the heats of formation for these perovskites and relate the data to their crystal structure. Furthermore, specific structural studies on the $Na_{1-x}Mg_xNb_{1-y}Ti_yO_{3-y}$ series are focused on determining the nature of the BO_6 octahedra.

Acknowledgment. The authors gratefully acknowledge M. Axness for her contributions to synthesis and characterization of samples and N. Ockwig, I. Levin, A. Ambrosini, and H. S. Kim for helpful discussions. Sandia is a multiprogram laboratory operated by Sandia Corporation, a Lockheed Martin Company, for the United States Department of Energy's National Nuclear Security Administration under Contract DE-AC04-94AL85000.

CM071122U

(27) Subbarao, E. C. *Solid Electrolytes and Their Applications*; Plenum Press: New York, 1980; p 9.